Published in final edited form as:

Langmuir. 2015 November 3; 31(43): 11858–11867. doi:10.1021/acs.langmuir.5b03473.

Nanoparticle Loaded Polymeric Microbubbles as Contrast Agents for Multimodal Imaging

Nutte Teraphongphom[†], **Peter Chhour**[‡,§], **John R. Eisenbrey**[‖], **Pratap C. Naha**[‡], **Walter R. T. Witschey**[‡,⊥], **Borirak Opasanont**[#], **Lauren Jablonowski**[†], **David P. Cormode**[‡,§], and **Margaret A. Wheatley**[†]

[†]School of Biomedical Engineering, Science and Health Systems, Drexel University, Philadelphia, Pennsylvania 19104 United States

[‡]Department of Radiology, University of Pennsylvania, Philadelphia, Pennsylvania 19104, United States

[§]Department of Bioengineering, School of Engineering and Applied Science, University of Pennsylvania, Philadelphia, Pennsylvania 19104, United States

[‖]Department of Radiology, Thomas Jefferson University, Philadelphia, Pennsylvania 19107, United States

[⊥]Department of Surgery, University of Pennsylvania, Philadelphia, Pennsylvania 19104, United States

[#]Chemical and Biological Engineering Department, Drexel University, Philadelphia, Pennsylvania 19104 United States

Abstract

Ultrasound contrast agents are typically microbubbles (MB) with a gas core that is stabilized by a shell made of lipids, proteins, or polymers. The high impedance mismatch between the gas core and an aqueous environment produces strong contrast in ultrasound (US). Poly(lactic acid) (PLA) MB, previously developed in our laboratory, have been shown to be highly echogenic both *in vitro* and *in vivo*. Combining US with other imaging modalities such as fluorescence, magnetic resonance imaging (MRI), or computerized tomography (CT) could improve the accuracy of many US applications and provide more comprehensive diagnostic information. Furthermore, our MB have the capacity to house a drug in the PLA shell and create drug-loaded nanoparticles *in situ* when passing through an ultrasound beam. To create multimodal contrast agents, we hypothesized that the polymer shell of our PLA MB platform could accommodate additional payloads. In this study, we therefore modified our current MB by encapsulating nanoparticles including aqueous or

Notes

The authors declare no competing financial interest.

NOTE ADDED AFTER ASAP PUBLICATION

This paper was published on the Web on October 16, 2015, prior to the galley corrections being made. The corrected version was reposted on October 20, 2015.

Supporting Information

The Supporting Information is available free of charge on the ACS Publications website at DOI: 10.1021/acs.langmuir.5b03473. Acoustic enhancement and acoustic stability data for all of the synthesized agents, a schematic depiction of the in vitro acoustic setup and a list of abbreviations are available (PDF)

organic quantum dots (QD), magnetic iron oxide nanoparticles (MNP), or gold nanoparticles (AuNP) to create bimodality platforms in a manner that minimally compromised the performance of each individual imaging technique.

Graphical Abstract

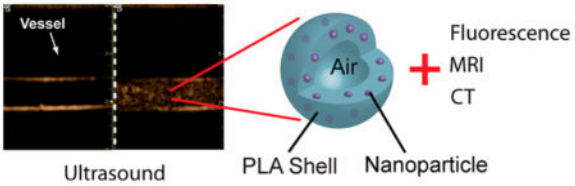

INTRODUCTION

Since the development of the first intravenous iodine-based contrast agents for X-ray imaging,[1] there has been tremendous progress in contrast agents, and now, these agents exist for many other types of imaging modalities, including magnetic resonance imaging (MRI), X-ray computed tomography (CT), ultrasound (US), and most recently photoacoustic imaging.[2–4] Each imaging modality has a unique mechanism of signal generation, which dictates the properties required of the contrast platform. For instance, most ultrasound contrast agents are microbubbles (MB) of less than 6 μm diameter, stabilized by a shell.[5,6] Ultrasound is strongly scattered because of the large difference in acoustic impedance between the suspending medium (blood) and the gas core of the microbubble.[7] The shell can be made from lipids, surfactants, or biocompatible, biodegradable polymers. The gas core is usually a dense, insoluble gas such as perfluorocarbon, or sulfur hexafluoride;[7] however, in our platform, we have developed an agent entrapping air.[8]

Currently, there is considerable interest in developing multimodal contrast agents.[9–11] Since each modality has its individual strengths and weaknesses, the use of complementary imaging modalities could be advantageous. Each modality can give different specifications to the images, for example, spatial and temporal resolution, sensitivity, and anatomical and molecular details, together with allowing different depths of penetration. Unique modality-specific details are provided, and in combination, a deeper understanding of the pathology can be obtained. A major advantage of multimodal agents lies in the fact that the injected agents will exhibit identical biodistribution and pharmacokinetics for each modality, allowing for superior cross-referencing between scans. In the field of multimodal contrast agents, a number of groups have loaded microbubbles with iron oxide nanoparticles to additionally provide contrast for MRI.[12,13] For example, Yang et al. have described nitrogen-filled double-layered microbubbles of poly(vinyl alcohol) (PVA) and poly(lactic acid) (PLA) encapsulating super-paramagnetic iron oxide (SPIO) nanoparticles.[11] Other PVA multimodal agents including poly(butyl cyanoacrylate) air-filled microbubbles have been used to encapsulate iron oxide particles for the combination of ultrasound and MRI.[14–19] Tartis et al. combined positron emission tomography (PET) and US with the use of ^{18}F-labeled lipid particles encapsulating a perfluorobutane core.[20] We have previously described MB composed of poly(lactic acid) and have demonstrated that drugs such as doxorubicin can be

incorporated into the polymer shell, with minimal compromise of the acoustic properties, indicating the potential of adding nanoparticle as a payload.[21] The acoustic properties of these new agents are expected to be influenced by inclusions of nanoparticles in the shell. For example, de Jong has modified the theoretical expression for acoustic cross-sectional area by including a shell elasticity term.[22] More recently, atomic force microscopy has been used to study the nanomechanical properties of biocompatible thin-shell hollow polymer microspheres.[23]

Such a multimodal imaging agent would have unique properties compared to those currently described in the literature. We have shown that as the MB pass through an ultrasound beam the bubbles resonate, and the pressure wave induces inertial cavitation. As a result, the MB shatter into fragments of less than 400 nm, which can be forced through leaky angiogenic tumor vessels into the interstitium of a tumor. This *in situ* nanofragment generation could now lead to multimodal imaging/nanoparticle delivery on the cellular level.[24]

In this study, we investigated quantum dots (QD), iron oxide magnetic nanoparticles (MNP), and gold nanoparticles (AuNP) loaded into our highly echogenic PLA, air-filled microbubbles platform.[25] QD are nanosized semiconductor crystals that are typically composed of two types of atoms from the II/VI or III/V group elements. These elements generate unique optical properties that have conferred advantages in bioanalytics over traditional fluorophores such as broad absorption, narrow excitation wavelengths, high quantum yield, low photobleaching, and resistance to chemical degradation.[26] These optical properties are tunable by the constituent materials, nanoparticle size, size distribution, and surface chemistry.[27] Magnetite (Fe_3O_4) or maghemite (γ-Fe_2O_3) are two types of iron oxide T_2* MRI contrast agents. MRI is widely used as a diagnostic tool for brain and central nervous system imaging, and for tumor detection. MRI can provide detailed anatomic images of soft tissue but lacks sensitivity. Both agents have an ability to dramatically shorten T_2* relaxation times.[28] AuNP have been studied as CT contrast agents.[29] CT is a commonly used, X-ray based, whole body imaging technique. AuNP have high X-ray absorption coefficients, low cytotoxicity, a surface chemistry that is easily tailored, biocompatibility, and surface plasmon resonance.[30]

We herein report the synthesis of these nanoparticle loaded microbubbles. The idealized configuration of QD, MNP or AuNP nanoparticles, incorporated into the polymer shell is illustrated in Figure 1. The microbubbles were characterized by electron microscopy, dynamic light scattering, zeta potential measurements, and elemental analysis. The nanoparticle loaded MB were tested for their fluorescence, CT, MRI, and US contrast generation. These experiments showed the agents to be functional for each modality. Preliminary cell viability measurements revealed the agents to be compatible with the cell lines studied. These agents can serve as true blood pool agents. Advantages of this platform are that the MB provides immediate, real-time, diagnostic information and that the functional multimodal polymeric platform can combine different information from each modalities for image fusion to increase accuracy in diagnostic treatment. The unique property of our microbubles to form *in situ* nanofragments when insonated opens up numerous future avenues to pursue.

EXPERIMENTAL SECTION

Materials

PLA (100 DL 7E (High IV)) was purchased from Evonik Industries AG (Darmstadt, Germany). PVA, 88% mole hydrolyzed, with a MW of 25 kDa was purchased from Polysciences (Warrington, PA). Ferrous chloride tetrahydrate (99%) ($FeCl_2{\cdot}4H_2O$), ferric chloride hexahydrate (99%) ($FeCl_3{\cdot}6H_2O$), ammonium hydroxide (25 wt % NH_3 in water) (NH_4OH), oleic acid (90%), gold chloride trihydrate (Au: 50%), dodecanethiol (98%), and Aliquat 336 were purchased from Sigma-Aldrich (St. Louis, MO, USA). CdS core and CdSe core QD (CS460 and CSE560) were purchased from NN-laboratories (Fayetteville, AR). All other chemicals were analytical grade from Fisher Scientific (Springfield, NJ), and used as received.

Synthesis of MNP

Oleic acid coated MNP were synthesized via precipitation with ammonia. Hydrophobic MNP were produced by an adaptation of a coprecipitation method.[31] Briefly, 5.8 g of $FeCl_3{\cdot}6H_2O$ and 2.15 g of $FeCl_2{\cdot}4H_2O$ were dissolved in 200 mL of DI water in a 250 mL Erlenmeyer flask under nitrogen gas for protection from oxidation, with vigorous magnetic stirring at 90 °C in a water bath. Then, 7.5 mL of NH_4OH was added dropwise into the suspension using a 25 mL syringe fitted with a 22G needle. This was followed by the addition of 4.5 mL of oleic acid in the same manner. After several minutes, a black magnetite gel precipitated at the bottom of the flask and was isolated by magnetic decantation. The magnetite gel was sonicated three times in acetone to remove excess oleic acid before dispersing in 10 mL of methylene chloride.

The synthesized MNP were characterized by transmission electron microscopy (TEM) to determine the average size and X-ray diffraction (XRD) to determine the crystal structure of iron oxide, magnetite (Fe_3O_4), or maghemite (γ-Fe_2O_3). XRD patterns were collected on a Rigaku SmartLab diffractometer equipped with a CuKα X-ray source generated at 40 kV and 44 mA in Bragg–Brentano mode with a CuKβ filter and a scanned angle from 20°–70°.

Synthesis of Gold Nanoparticles

AuNP were synthesized using two-phase reduction as per the method of Brust.[32] Chloroauric acid (5.06 g (12.8 mM)) was dissolved in 50 mL of Milli-Q water. To this was added 8.31 g (20.6 mM) of methyl trioctylammonium chloride (Aliquat 336) in 50 mL of toluene. The mixture was stirred for 2 h before the now orange organic layer was removed. This organic layer, with 50 mL more of toluene added, was stirred in an ice bath. Dodecanethiol (0.153 mL (0.64 mM)) was added to the solution. Then, 19.37 g (512 mM) of sodium borohydride in 50 mL of Milli-Q water was added dropwise. The solution turned inky black. After 1 h, the organic layer was separated, washed twice with 50 mL of Milli-Q water, an excess (6.14 mL) of dodecanethiol was added, and the solution was allowed to stir overnight. The volume was then reduced to 10 mL, 400 mL of methanol was added, and solution was cooled to −23 °C for 16 h. The nanoparticle suspension was filtered, and the resulting nanoparticles were washed with 50 mL each of acetone, acetonitrile, ethanol, and

methanol. The washing step was repeated to yield a waxy black solid, which was dried under vacuum prior to use

Fabrication of Microbubbles

The method for entrapment of the nanoparticles within the wall of polymeric MB is an adaptation of the method previously developed within our laboratory to produce unloaded PLA MB using a double emulsion evaporation technique (w/o/w).[25]

The different loading concentrations for each nanoparticle synthesis are summarized in Table 1 where the loading is expressed as the total nanoparticle weight (core and coating) as a percentage of the PLA weight used. Methods used for drug-loaded ultrasound contrast agents were adapted for the synthesis of multimodal agents, taking into account the nature of the nanoparticle being encapsulated. Briefly, 0.5 g of PLA and 0.05 g of camphor were dissolved in 10 mL of methylene chloride. To make organic QD-MB, MNP-MB, and AuNP-MB, the respective nanoparticles were added individually into this polymer mixture and magnetically stirred. After fully dispersing the nanoparticles, 1 mL of 0.4 M aqueous ammonium carbonate ($(NH_4)_2CO_3$) was added to the polymer mixture. In the original method, a synergistic effect on echogenicity was noted with the use or dual porogens, one in the organic phase (camphor) and one in the aqueous phase ($(NH_4)_2CO_3$). For aqueous QD-MB synthesis, aqueous QD were added to the $(NH_4)_2CO_3$ solution prior to addition to the dissolved polymer solution. The methylene chloride/aqueous mixture in all cases was sonicated at 20 kHz using 110 W of applied power for 30 at 3 s on, 1 s off (Misonix Inc. CL4 tapped horn probe with 0.5″ tip, Farmingdale, NY) while suspended in an ice bath. The resulting (W/O) emulsion was added to 50 mL of cold 5% aqueous PVA as the second water phase and homogenized for 5 min at 9600 rpm (Brinkmann Instruments, Westbury, NY). After homogenization, the resulting water-in-oil-in-water (W/O/W) emulsion was added to 100 mL of 2% isopropyl alcohol. Samples were then continually stirred in a fume hood for 1 h to evaporate any organic solvent. Following evaporation, MB were collected using centrifugation at 5000 rpm (relative centrifugal force 2600*g*) for 5 min and washed three times with 5 mL of hexane each. The capsules were left inside a fume hood to evaporate hexane. Then, MB were flash frozen with liquid nitrogen and lyophilized for 48 h to create a hollow core inside by subliming ammonium carbonate and camphor which was filled in with air once the vacuum was released.

Size, Morphology, and Concentration Characterization

Dynamic Light Scattering—The microbubbles were characterized using a dynamic light scattering (DLS) particle size analyzer (ZetaSizer Nano ZS Particle Size Analyzer, Malvern, MA) to determine average diameter and size distribution represented by the polydispersity index (PDI). Samples were prepared by mixing MB with PBS at a concentration of 1 mg/mL. The suspension was pipetted into a plastic cuvette and measured using the analyzer at room temperature. Zeta potential (ζ) measurements were made on the same instrument to monitor any change in surface charge. For ζ measurement, the MB was resuspended in DI water at the same concentration as that for size determination, and the suspension was pipetted into a Malvern Zeta capillary cuvette.

Concentration—Microbubble counting was performed using a flow cytometer, LSRII (BD Biosciences, San Jose, CA). Samples were prepared by mixing in DI water at the concentration of 20 μg/mL. Then, 0.5 mL of the vortexed suspension was added to 10 μL of UV Countbright absolute counting beads (containing 9800 beads used as a counting standard; Life Technologies, Grand Island, NY). Counting beads and MB were separated using Forward Scatter A and Phycoerythrun-A filters.

Scanning Electron Microscope and Transmission Electron Microscopy

A scanning electron microscope (SEM) (Zeiss Supra 50VP) was used to assess the MB surface morphology. Images were taken at high vacuum mode with varying magnifications at an accelerating voltage of 5.0 kV. All SEM imaging was done at the Drexel University Materials Characterization Facility. Transmission electron microscopy (TEM) (JEM 1010, JEOL) was performed at an accelerating voltage of 80 kV to investigate the microstructure of the agents. The samples were prepared by drop-casting the sample dispersion onto a Formvar film copper grid. The grid was placed on filter paper to absorb excess solvent.

Fluorescence Imaging

Confocal fluorescence microscopy was used for visualization of QD within MB and to establish that the fluorescent properties of QD are still retained at the same absorption and emission frequencies. Confocal microscopy was performed using an Olympus IX81microscope run by Olympus Fluorview version 1.7b (Olympus Corporation, Tokyo). One milligram of each QD-MB was mixed with 1 mL of PBS and a droplet was placed on a glass microscope slide. The MB were observed at 100× magnification with the use of microscope oil immersion.

Nanoparticle Encapsulation Efficiency and Loading Percentages

Amounts of encapsulated QD were determined by dissolving 2 mg of dry MB in 2 mL of DMSO vortexing for 30 s to dissolve the polymer and measuring the fluorescent intensity of the resulting solution using a Tecan fluorimeter (Männedorf, Switzerland). QD concentration was then calculated based on a standard curve of known amounts of QD in DMSO. Encapsulated MNP and AuNP were determined by inductively coupled plasma-optical emission spectroscopy (ICP-OES) on a Spectro Genesis system (Kleve, Germany). Samples were dissolved in 5% aqua regia (3:1 HCl:HNO_3) before analysis.

In Vitro Acoustic Testing and Stability

To assess the acoustic properties of the various contrast agents, acoustic enhancement and stability in an US beam were assessed. Backscattering enhancement of all fabricated MB was determined using an *in vitro* custom-built acoustic setup (an illustration of the setup is displayed in Figure S1, Supporting Information). The enhancement measurement is shown as a function of MB dosage and used to determine the ability of the sample to provide enhancement.

A transducer with a centered frequency of 5-MHz, 12.7 mm diameter, −6 dB bandwidth of 91%, and focal length of 50.8 mm, and a pulselength of 1 μs, was used to both transmit and receive signals. The transducer was placed in a 37 °C water bath and focused through the

acoustically transparent window of an acrylic sample holder containing 50 mL of 37 °C phosphate buffered saline (PBS) at pH 7.4 to simulate body fluid environment. A pulser/receiver (Panametrics Waltham, MA) was used to generate an acoustic pulse with a pulse repetition frequency (PRF) of 100 Hz. Microbubbles in the sample holder were insonified with pulses having a peak negative pressure of 0.45 MPa (equivalent to MI = 0.09). Pressure calibration was done with a 0.5 mm polyvinylidene fluoride needle hydrophone (Precision Acoustics, Dorset, UK), as previously published.[33] The scattered signal was amplified 40 dB by the receiver then displayed by an oscilloscope (Lecroy 9350 A Chestnut Ridge, NY). Labview 13 (National Instruments, Austin, TX) was used for data acquisition and processing. Prior to the addition of MB into the sample holder, baseline readings were taken to measure the background signal. Then, 20 μL of the MB suspension made from mixing 3 mg of MB into 800 μL of PBS was added to the sample holder, and the cumulative acoustic signal was recorded. Acoustic backscattering enhancement was defined as

$$\text{acoustic enhancement} = 20\log\left(\frac{\text{rms[MB]}}{\text{rms[Blank]}}\right)$$

where rms[MB] is the root-mean-square of the backscattered signal measured after the MB was added, and rms[Blank] is the root-mean-square of the backscattered signal measured before the addition of MB.

The same acoustic model was also used to determine the stability of the MB in providing contrast throughout an average of 15–20 min duration of a typical US scan. The sample was continuously stirred and insonicated for 15 min. Doses of MB on the rise of the dose–response curve close to the plateau were used to avoid measuring an exaggerated stability. The results were normalized by the enhancement at the first dosage to allow for intersample comparison. All measurements were repeated in triplicate for each of three separate samples (6 readings, $n = 2$).

Ultrasound Phantoms Imaging

Apart from acoustic enhancement analysis, MB underwent testing with a commercial US scanner (Logiq 9 US scanner) with a 9 L probe operating in nonlinear contrast imaging mode (GE Healthcare, Milwaukee, WI). A bolus injection of 1.0×10^7 microbubbles was determined from the result obtained by *in vitro* acoustic testing to give good images for the duration of the scan for all formulas except for AuNP-MB which were deemed from the *in vitro* acoustic testing to be higher, at 1.0×10^{11} microbubbles. Bubbles were injected into 800 mL of PBS that was circulated through a flow phantom (model 524; ATS Laboratories, Bridgeport, CT) with a 6 mm diameter vessel embedded at a depth of 2 cm in urethane rubber using a roller pump set at 350 mL/min. Ultrasound images were captured for every minute post injection for 15 min.

Relaxometry, CT, and MRI Phantoms Imaging

The MRI relaxation times of MNP-MB were determined with relaxometry (1.41 T, 60 MHz, 40 °C, Minispec, Bruker) by encapsulating the MNP-MB in 1% agarose gel. The

concentrations used were 0.033, 0.167, 0.250, 0.334, 0.583, and 0.834 mM Fe. Phantom MRI of MNP-MB was carried out at various iron concentrations from 0 mM to 0.32 mM (0, 0.016, 0.032, 0.081, 0.16, 0.24, and 0.32 mM Fe), i.e., 1.56×10^7 microbubbles/mL. Phantom scanning was performed on a clinical 3 T MRI scanner (Tim Trio, Siemens Healthcare, Erlangen, Germany). T_2-weighted images were obtained using a spin echo sequence with the following imaging parameters: TR = 10 s, FOV = 100 × 140 mm^2, slice thickness = 3 mm, in plane spatial resolution = 0.546 mm^2, matrix size = 184 × 256, bandwidth = 592 Hz/pixel, excitation flip angle = 90°, refocusing flip angle = 180°. Ten TEs were measured from TE = 6.5–40 ms.

The CT attenuation rate of AuNP-MB was determined using a clinical scanner, as previously described.[34] In short, different concentrations of AuNP-MB (2.5, 5.0, 20.0, 25.0, 38.0, and 51.0 mM Au) were dispersed in 1% agarose gel, and the samples placed into a tank of water (21 cm in height and 24 cm in width) to simulate being in the body. Imaging was performed using a 64-slice scanner (Definition DS, Siemens Medical Solutions, Malvern, PA) in single source acquisition mode at 120 kV and 300 mA with a matrix of 512 × 512, field of view of 37 × 37 cm, and a slice thickness of 0.6 cm. The reconstruction kernel used was B30f. Images were analyzed using Osirix 64 bit (v3.7.1). The attenuation was analyzed by placing an ROI in each tube in three separate slices. The values were averaged, and the attenuation rate ($HU_{25–100}$/mM)[35] was calculated from the slope of the line from the linear fit of plots of attenuation vs concentration.

Cell Culture

The mouse monocytes, RAW 264.7 (ATCC, Manassas, VA, USA), were cultured in Dulbecco's modified Eagle's medium (DMEM) supplemented with 10% fetal bovine serum and 1% penicillin/streptomycin (10,000 units/mL, 10,000 μg/mL) from Life Technologies Invitrogen (Grand Island, NY). Human liver hepatocellular cell line HepG2 (ATCC) was grown in Eagle's minimal essential medium (EMEM) supplemented with 10% fetal bovine serum and 1% penicillin/streptomycin (10,000 units/mL, 10,000 μg/mL). The cells were maintained in a humidified incubator at 37 °C in a 5% CO_2 atmosphere.

Cell Viability

All agents were tested in tissue culture. Cells were cultured on glass bottomed dishes at 0.5 M cells/cm for 24 h. Afterwards, the cells were incubated with conditioned medium containing 0.5 mg of agents per mL of medium for 4 h. Unloaded agent and nontreated cells (media only) were used as control groups. After 4 h, the medium was removed, and cells were washed with DPBS, and their viability was evaluated using a Live/Dead Cytotoxicity Assay (Invitrogen, NY).

Statistical Analysis

All measurements were repeated in triplicate for each of three separate samples (6 readings, $n = 2$). Statistical significance for multiple groups was assessed using a one-way analysis of variance, and individual groups were compared using Student's t test ($a = 0.05$) using Graphpad Prism 6 (San Diego, CA). Values are reported as the mean. Error bars were displayed as standard error about the mean.

RESULTS AND DISCUSSION

Nanoparticle Characterization

Both AuNP and MNP were synthesized and characterized prior to loading into the MB platform. After synthesis of MNP by the precipitation method, the samples were subjected to X-ray powder diffraction measurements to identify the crystal structure. The XRD diffractogram of the synthesized MNP is displayed in Figure 2. The profile is consistent with that of Fe_3O_4 crystals based on comparison with the standard pattern of Fe_3O_4.

TEM images of free QD (aqueous and organic), MNP, and AuNP are shown in Figure 3, first row. Aqueous QD, organic QD, and AuNP were found to be monodispersed in size and shape by TEM. MNP were relatively more polydispersed with an average diameter of 10 nm. The properties of each nanoparticle type used in this study are displayed in Table 2. Average sizes of QD were obtained from the manufacturer. AuNP and MNP were determined by TEM, and the average sizes are also shown on Table 2.

Multimodal Platform Development

The completed syntheses resulted in purple, orange, and white powders for the gold, iron oxide, and quantum dots, respectively. The coloration acted as an initial indication that the nanoparticle had been loaded into the MB. We subsequently characterized the formulations, with respect to their individual contrast properties.

As seen in the second and third row of Figure 3, organic QDs, MNP, and AuNPs were found to be encapsulated inside the shell of the microbubble. This is evident from the diffuseness of the nanoparticles throughout the shell of the microbubble. In the MB preparation, aqueous QD are loaded in the first water phase which, in a standard w/o/w emulsion, becomes the inner phase when the first w/o emulsion is added to a large volume of the second aqueous phase. If the QD remain associated with the first aqueous phase, then it is likely that they become attached to the inside of the shell upon removal of the water upon freeze-drying. The location difference of the organic QDs, MNP, and AuNPs as compared to aqueous QD can be attributed to the hydrophobicity of the coatings. The hydrophobic particles are loaded into the MB with an organic polymer mixture while the aqueous nanoparticles are mixed with a $(NH_4)_2CO_3$ solution during synthesis. Although, the hydrophobic coated nanoparticles are similarly loaded within the shell, the organization for nanoparticle type differs as seen in the high magnification TEM images. Organic QD and AuNP appear to be arranged in clusters within the shell as opposed to uniform dispersion for the loading of MNP. The different behaviors observed for the QD and AuNP can be partially attributed to the different surface properties among the nanoparticles, which influence the formation of the aggregates during the emulsion process resulting in clusters of QD and AuNP in the outer shell of the MB.

The high magnification images of these MB are shown in the third row of Figure 3. These TEM images revealed that both types of QD and AuNP are aggregated, unlike the MNP that have uniform dispersion of nanoparticle in the shell of the MB. The aggregations occurred independent of different loading percent values of the nanoparticles.

MB size, polydispersity index (PDI), and ζ were measured for samples made with increasing nanoparticle load to determine if encapsulating nanoparticles in the shell of MB would significantly alter the physical characteristics of the samples. However, the MB characteristics were consistent for both high and low loadings of the same kind of nanoparticles; therefore, we determined that the amount of nanoparticles was not a major factor that modifies the shell characteristics. Hence, only representative results for the highest loadings of each nanoparticle are shown in Table 3. Nanoparticle loading into the shell had no effect on PDI or ζ. Only incorporation of AuNP-MB had a significant effect on the size of MB ($p = 0.0213$), which was decreased in comparison to that of the unloaded MB. The lack of effect on ζ is expected, given that the nanoparticle should be internalized in the polymer shell and not at the surface of the hydrophobic QD. For the hydrophilic QD, the surface loading observed was fairly low, which is consistent with the minor change in ζ. A large negative ζ of all MB also indicates that the MB are likely to repel each other resulting in a lower chance of flocculating. Concentrations of each sample are shown in Table 3. Because of the loading of the nanoparticle inside the shell of the MB, the concentrations of the loaded MB are all lower compared with the blank MB (2.5×10^9 microbubbles/mg).

Figure 4 shows SEM images of the different MB formulations. As can be seen, loading the different nanoparticles into MB did not significantly affect gross surface morphology. The images show that the nanoparticle loaded MB appear to have smooth surfaces and retain their spherical shape. The SEMs show that the nanoparticle entrapped MB have size distributions between 1 and 3 μm, which is consistent with the data obtained from dynamic light scattering measurements. MB sizes larger than 8 μm would represent a safety concern for biomedical applications. As can be seen from Figure 4, no MBs were larger than 3 μm, indicating the safety of the formulation from a size perspective.

Figure 5 shows the results of confocal microscopy examination of QD-MB. Each of the QD-MB formulations was fluorescent when excited at their respective excitation peaks. Although the TEM images of the QD-MB show scattered distribution of the QD inside the shell of the microbubble, the fluorescent image quality does not seem to be affected, and the spherical shape of QD-MB can still be observed. Hence, the fluorescent properties of both types of QD were retained when loaded into MB. It may be noted that the MB appear larger in the fluorescence microscopy images than was determined by SEM measurement; however, fluorescence microscopy is not a precise method to determine particle size; therefore, we view the SEM measurements as reliable.

Loading Efficiency

After determining the amount of each nanoparticle in gram/gram final agent, the percentage yield, loading, and encapsulation efficiency were defined in eqs 1 – (3):

$$\text{wt \% yield} = \frac{\text{final total MB weight}}{\text{total initial weight of polymer and nanoparticle}} \times 100 \quad (1)$$

$$\text{wt \% loading} = \frac{\text{final nonoparticle weight}}{\text{total MB weight}} \times 100 \quad (2)$$

$$\text{wt \% encapsulation efficiency} = \frac{\text{final nanoparticle weight}}{\text{initial nanoparticle weight}} \times 100 \quad (3)$$

Table 4 summarizes the percentage yield, loading, and encapsulation efficiency of the highest loaded microbubble samples tested for each nanoparticle. Aqueous QD-MB exhibited the lowest encapsulation efficiency of 10.5% ± 0.65 compared with that of the other types of nanoparticles. This is consistent with our previous findings comparing the encapsulation of the hydrophobic paclitaxel and hydrophilic doxorubicin in PLA MB.[33] This might result from the different loading step of aqueous QD-MB compared with the other, hydrophobically coated nanoparticle.

In Vitro Acoustic Testing and Stability

Effects of MB dose, nanoparticle type, and loading on acoustic properties as measured *in vitro* by a dose–response curve were examined. Figure 6 shows the results of both backscattering enhancement as a function of MB dose (A) and acoustic stability over time (B). The cumulative dose–responses of the MB with the highest loadings of the different nanoparticles are shown in Figure 6A and are compared with the unloaded MB as a control group (data for all formulations are displayed in Figure S2). Except for AuNP-MB (p = 0.0130), there was no statistical difference between the various agents ($p > 0.05$) compared with the blank MB, which all reached enhancements of 17–18 dB at doses of 5×10^6 number of MB/mL and above. This value is acceptable for good *in vivo* imaging.[8] In the case of the AuNP-MB, the acoustic enhancement was lower, but by increasing in concentration, the acoustic enhancement would gradually reach the same level as the control group; however, they are still effective contrast agents as shown in the ultrasound flow phantom section. This discrepancy could be due to either the AuNP altering the shell acoustic properties by reinforcing the polymer shell and increased the elastic modulus[15] or the smaller size of the AuNP-MB.

In Figure 6B, the acoustic stability of all nanoparticle loaded MB remained in the same range as that of the control MB, and all agents lose roughly 35% of their original enhancement after 15 min of insonation under these conditions. Thus, they are able to provide enhancement half-lives longer than 20 min. Overall, these results suggest that the addition of nanoparticle to the shell of the MB does not significantly affect the acoustic performance of MB and indicate that the agents are still capable of functioning as ultrasound contrast agents that shatter when exposed to US.

In Figure 7, the nanoparticle loaded MB were tested with a commercial US scanner (nonlinear contrast imaging mode on the right-sided of split screen in gold). The flow phantom images of the 6 mm vessel lumen at a depth of 2 cm show strong enhancements post-injection (t = 15 min) on the right column compared to the baseline on the left column.

The bubbles show high contrast activity even after 15 min. This indicates that the MB are suitable as ultrasound contrast agents.

Relaxometry

The 50.0 wt % MNP-MB formulation was investigated for its ability to act as an MRI contrast agent by assessing its longitudinal (r_1) and transverse (r_2) relaxivities. The relaxivity of MNP is defined as the efficiency to enhance the relaxation rate of the neighboring water protons and is expressed in $s^{-1}mM^{-1}$. The contrast agent can be determined to operate best as a T_1 (spin–lattice relaxation time) or T_2 (spin–spin relaxation time) contrast agent. Generally, MNP are used in T_2-weighted MR imaging. The r_1 was found to be 1.7 $s^{-1}mM^{-1}$and r_2 to be 118 $s^{-1}mM^{-1}$; thus, the r_2/r_1 is 70.77. The large r_2 value and high r_2/r_1 value indicates that the agent should be effective for T_2- or T_2*-weighted imaging.

MRI and CT Phantom Imaging

MR images from a phantom of several concentrations of MNP-MB are shown in Figure 8 (upper row). As can be seen, the MRI signal decreased as the concentration of the MNP-MB increased, providing further evidence that MNP-MB can be used as a MRI contrast agent. The highest MNP concentration at 0.324 mM is equivalent to 1.56×10^7 microbubbles/mL. Phantom images of a range of concentrations of 50.0 wt % AuNP-MB acquired with a clinical CT scanner are shown in Figure 8 (lower row). A concentration dependent (highest at 51 mM of AuNP, which is equivalent to 3.17×10^9 microbubbles/mL) increase in the contrast produced by the agent is readily apparent from the images. The CT attenuation rate of the agent was determined from this data set to be 5.8 ($HU_{25–100}$/mM).[35] This value is comparable to those previously determined for gold nanoparticles.[29] The higher concentrations used for CT are due to the lower sensitivity of CT, compared with that of MRI.

Cell Viability

Initial *in vivo* tests of the MB targeted the liver and were directed at hepatocellular carcinoma.[36] For reference, we tested the effects of our agents on hepatocyte (HepG2) and macrophage (RAW 264.7) related cell lines, the cell types of which the liver is mostly composed. After 4 h of incubation with nanoparticle loaded MB, cell viability was measured with the Live/Dead assay to determine any cytotoxic effect of the agents on the cell lines (Figure 9). Both the loaded MB and unloaded MB were not seen to statistically reduce cell viability for either the RAW 264.7 or HepG2 cell lines compared to that of the control (media only) ($p > 0.05$). Therefore, we can conclude that all agents are biocompatible under the conditions tested. While toxicity might be found at higher concentrations, we used a concentration of 0.5 mg polymer/mL, roughly 50 times the clinically used peak concentration in blood for currently approved ultrasound contrast agents or 75 times the dose expected in the liver;[36] therefore, these agents would be biocompatible within the relevant concentration range.

CONCLUSIONS

In this study, we have shown that the QD, MNP, and AuNP nanoparticles can be encapsulated inside a PLA microbubble and that the resulting multimodal platforms retain their individual contrast properties without adversely compromising US enhancement or stability. The contrast observed in CT, MRI, and fluorescence images acquired using nanoparticle loaded MB shows that the polymeric MB containing secondary imaging agents have potential for being used as dual mode contrast agents to monitor a targeted tumor site. For example, the AuNP-MB would provide contrast for CT, a whole body technique, while providing contrast in ultrasound imaging, which would offer soft tissue contrast and real-time imaging. This family of MB could provide an improved platform technology for various dual-imaging approaches but, more significantly, present a possible platform for multimodal imaging with concomitatnt *in situ* generation of drug-loaded microbubble fragments.

Supplementary Material

Refer to Web version on PubMed Central for supplementary material.

Acknowledgments

We thank A.J. Drexel Nanotechnology Institute (DNI) for the use of the confocal microscope and Dr. Lei Yu from Thomas Jefferson University's Flow Cytometry Core Facility for assistance with the flow cytometry system. This work was supported by SIR Foundation Allied Scientist Grant, NIH grants R00 EB012165 (to D.P.C.) and R00 HL108157 (to W.R.T.W.), and via start up funds from the University of Pennsylvania (to D.P.C.).

References

1. Idée, J-M.; Nachman, I.; Port, M.; Petta, M.; Lem, GL.; Greneur, SL.; Dencausse, A.; Meyer, D.; Corot, C. Iodinated Contrast Media: From Non-Specific to Blood-Pool Agents. In: Krause, PDW., editor. Contrast Agents II. Springer; Berlin, Germany: 2002. p. 151-171.Topics in Current Chemistry
2. Bornhop DJ, Contag CH, Licha K, Murphy CJ. Advances in Contrast Agents, Reporters, and Detection. J Biomed Opt. 2001; 6:106–110. [PubMed: 11405205]
3. Mattrey RF, Aguirre DA. Advances in Contrast Media Research 1. Acad Radiol. 2003; 10:1450–1460. [PubMed: 14697013]
4. Mattrey RF. Blood-pool Contrast Media Are the Ideal Agents for Computed Tomography. Invest Radiol. 1991; 26(Suppl 1):S55–S56. discussion S60–S64. [PubMed: 1808150]
5. Balen FG, Allen CM, Lees WR. Ultrasound Contrast Agents. Clin Radiol. 1994; 49:77–82. [PubMed: 7907285]
6. Calliada F, Campani R, Bottinelli O, Bozzini A, Sommaruga MG. Ultrasound Contrast Agents: Basic Principles. Eur J Radiol. 1998; 27(Suppl 2):S157–S160. [PubMed: 9652516]
7. Klibanov AL. Preparation of Targeted Microbubbles: Ultrasound Contrast Agents for Molecular Imaging. Med Biol Eng Comput. 2009; 47:875–882. [PubMed: 19517153]
8. Wheatley MA, Forsberg F, Oum K, Ro R, El-Sherif D. Comparison of in Vitro and in Vivo Acoustic Response of a Novel 50:50 PLGA Contrast Agent. Ultrasonics. 2006; 44:360–367. [PubMed: 16730047]
9. Al-Jamal WT, Al-Jamal KT, Bomans PH, Frederik PM, Kostarelos K. Functionalized-Quantum-Dot–Liposome Hybrids as Multimodal Nanoparticles for Cancer. Small. 2008; 4:1406–1415. [PubMed: 18711753]

10. Liao Z, Wang H, Wang X, Zhao P, Wang S, Su W, Chang J. Multifunctional Nanoparticles Composed of A Poly(Dl-lactide-coglycolide) Core and A Paramagnetic Liposome Shell for Simultaneous Magnetic Resonance Imaging and Targeted Therapeutics. Adv Funct Mater. 2011; 21:1179–1186.
11. Yang F, Li Y, Chen Z, Zhang Y, Wu J, Gu N. Superparamagnetic Iron Oxide Nanoparticle-embedded Encapsulated Microbubbles as Dual Contrast Agents of Magnetic Resonance and Ultrasound Imaging. Biomaterials. 2009; 30:3882–3890. [PubMed: 19395082]
12. Fokong S, Theek B, Wu Z, Koczera P, Appold L, Jorge S, Resch-Genger U, van Zandvoort M, Storm G, Kiessling F, et al. Image-guided, Targeted and Triggered Drug Delivery to Tumors Using Polymer-based Microbubbles. J Controlled Release. 2012; 163:75–81.
13. Liu Z, Lammers T, Ehling J, Fokong S, Bornemann J, Kiessling F, Gätjens J. Iron Oxide Nanoparticle-containing Microbubble Composites as Contrast Agents for MR and Ultrasound Dual-modality Imaging. Biomaterials. 2011; 32:6155–6163. [PubMed: 21632103]
14. Sciallero C, Trucco A. Ultrasound Assessment of Polymer-shelled Magnetic Microbubbles Used as Dual Contrast Agents. J Acoust Soc Am. 2013; 133:EL478–484. [PubMed: 23742443]
15. Poehlmann M, Grishenkov D, Kothapalli SVVN, Härmark J, Hebert H, Philipp A, Hoeller R, Seuss M, Kuttner C, Margheritelli S, et al. On the Interplay of Shell Structure with Low- and High-frequency Mechanics of Multifunctional Magnetic Microbubbles. Soft Matter. 2014; 10(10): 214–226. [PubMed: 24651844]
16. Poepping TL, Nikolov HN, Thorne ML, Holdsworth DW. A Thin-walled Carotid Vessel Phantom for Doppler Ultrasound Flow Studies. Ultrasound Med Biol. 2004; 30:1067–1078. [PubMed: 15474751]
17. Park JI, Jagadeesan D, Williams R, Oakden W, Chung S, Stanisz GJ, Kumacheva E. Microbubbles Loaded with Nanoparticles: A Route to Multiple Imaging Modalities. ACS Nano. 2010; 4:6579–6586. [PubMed: 20968309]
18. He W, Yang F, Wu Y, Wen S, Chen P, Zhang Y, Gu N. Microbubbles with Surface Coated by Superparamagnetic Iron Oxide Nanoparticles. Mater Lett. 2012; 68:64–67.
19. Lin CAJ, Chuang WK, Huang ZY, Kang ST, Chang CY, Chen CT, Li JL, Li JK, Wang HH, Kung FC, et al. Rapid Transformation of Protein-Caged Nanomaterials into Microbubbles As Bimodal Imaging Agents. ACS Nano. 2012; 6:5111–5121. [PubMed: 22607131]
20. Tartis MS, Kruse DE, Zheng H, Zhang H, Kheirolomoom A, Marik J, Ferrara KW. Dynamic microPET Imaging of Ultrasound Contrast Agents and Lipid Delivery. J Controlled Release. 2008; 131:160–166.
21. Eisenbrey JR, Burstein OM, Kambhampati R, Forsberg F, Liu JB, Wheatley MA. Development and Optimization of a Doxorubicin Loaded Poly(lactic Acid) Contrast Agent for Ultrasound Directed Drug Delivery. J Controlled Release. 2010; 143:38–44.
22. Frinking PJ, de Jong N. Acoustic Modeling of Shell-encapsulated Gas Bubbles. Ultrasound Med Biol. 1998; 24:523–533. [PubMed: 9651962]
23. Glynos E, Koutsos V, McDicken WN, Moran CM, Pye SD, Ross JA, Sboros V. Nanomechanics of Biocompatible Hollow Thin-Shell Polymer Microspheres. Langmuir. 2009; 25:7514–7522. [PubMed: 19379000]
24. Cochran MC, Eisenbrey JR, Soulen MC, Schultz SM, Ouma RO, White SB, Furth EE, Wheatley MA. Disposition of Ultrasound Sensitive Polymeric Drug Carrier in a Rat Hepatocellular Carcinoma Model. Acad Radiol. 2011; 18:1341–1348. [PubMed: 21971256]
25. El-Sherif DM, Wheatley MA. Development of a Novel Method for Synthesis of a Polymeric Ultrasound Contrast Agent. J Biomed Mater Res. 2003; 66:347–355.
26. Medintz IL, Uyeda HT, Goldman ER, Mattoussi H. Quantum Dot Bioconjugates for Imaging, Labelling and Sensing. Nat Mater. 2005; 4:435–446. [PubMed: 15928695]
27. Subramaniam P, Lee SJ, Shah S, Patel S, Starovoytov V, Lee KB. Generation of a Library of Non-Toxic Quantum Dots for Cellular Imaging and siRNA Delivery. Adv Mater. 2012; 24:4014–4019. [PubMed: 22744954]
28. Iida H, Takayanagi K, Nakanishi T, Osaka T. Synthesis of Fe3O4 Nanoparticles with Various Sizes and Magnetic Properties by Controlled Hydrolysis. J Colloid Interface Sci. 2007; 314:274–280. [PubMed: 17568605]

29. Cormode DP, Naha PC, Fayad ZA. Nanoparticle Contrast Agents for Computed Tomography: a Focus on Micelles. Contrast Media Mol Imaging. 2014; 9:37–52. [PubMed: 24470293]

30. Mieszawska AJ, Mulder WJM, Fayad ZA, Cormode DP. Multifunctional Gold Nanoparticles for Diagnosis and Therapy of Disease. Mol Pharmaceutics. 2013; 10:831–847.

31. Liu X, Kaminski MD, Chen H, Torno M, Taylor L, Rosengart AJ. Synthesis and Characterization of Highly-magnetic Biodegradable Poly(d,l-lactide-co-glycolide) Nanospheres. J Controlled Release. 2007; 119:52–58.

32. Brust M, Walker M, Bethell D, Schiffrin DJ, Whyman R. Synthesis of Thiol-derivatised Gold Nanoparticles in a Two-phase Liquid–Liquid System. J Chem Soc, Chem Commun. 1994:801–802.

33. Cochran MC, Eisenbrey J, Ouma RO, Soulen M, Wheatley MA. Doxorubicin and Paclitaxel Loaded Microbubbles for Ultrasound Triggered Drug Delivery. Int J Pharm. 2011; 414:161–170. [PubMed: 21609756]

34. Galper MW, Saung MT, Fuster V, Roessl E, Thran A, Proksa R, Fayad ZA, Cormode DP. Effect of Computed Tomography Scanning Parameters on Gold Nanoparticle and Iodine Contrast. Invest Radiol. 2012; 47:475–481. [PubMed: 22766909]

35. Cormode DP. Letter to the Editor Re: Spectral Hounsfield Units – A New Radiological Concept. Eur Radiol. 2013; 23:640–641. [PubMed: 22971961]

36. Willmann JK, Cheng Z, Davis C, Lutz AM, Schipper ML, Nielsen CH, Gambhir SS. Targeted Microbubbles for Imaging Tumor Angiogenesis: Assessment of Whole-Body Biodistribution with Dynamic Micro-PET in Mice. Radiology. 2008; 249:212–219. [PubMed: 18695212]

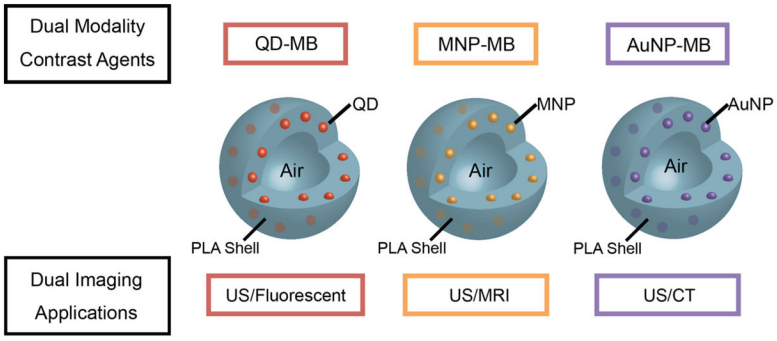

Figure 1.
Schematic depiction of idealized nanoparticle loaded MB.

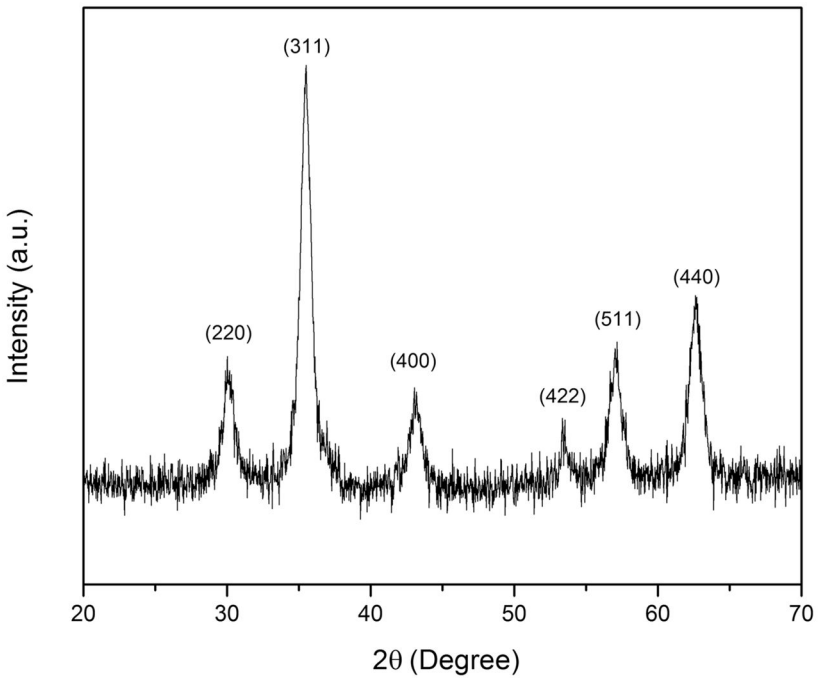

Figure 2.
XRD diffractogram of MNP synthesized via a coprecipitation method.

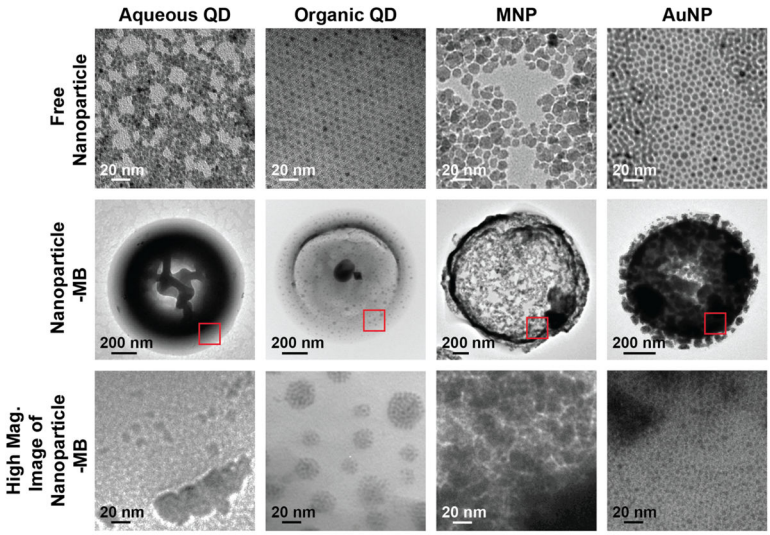

Figure 3.
TEM images of free nanoparticle, nanoparticle-MB, and high magnification images of nanoparticles embedded in the MB.

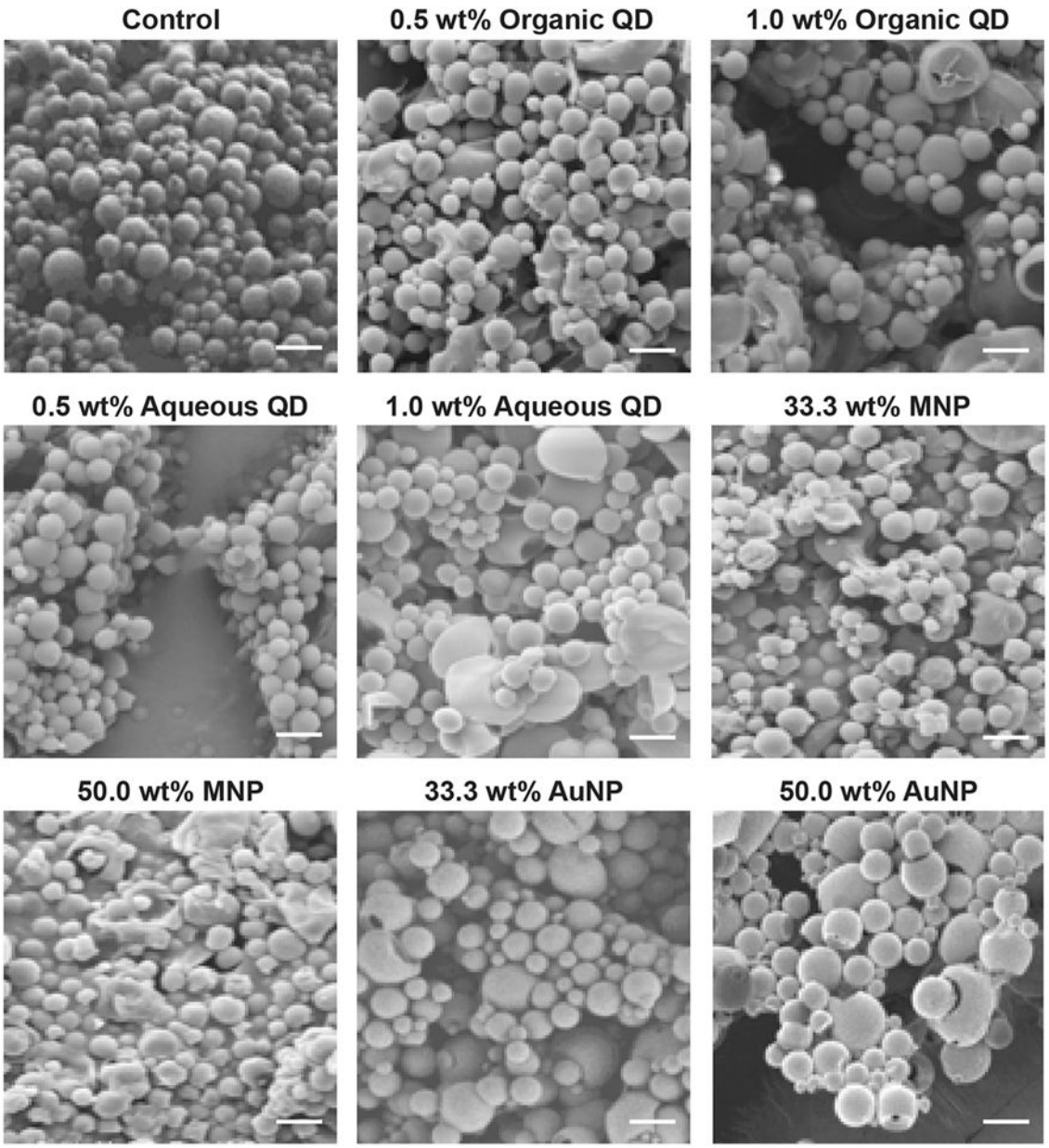

Figure 4.

SEM images of MB. Accelerating voltage is 3 kV. Spot size is 3. Magnification is 3.5 kX. The scale bar is the same in each panel and is 2.5 μm.

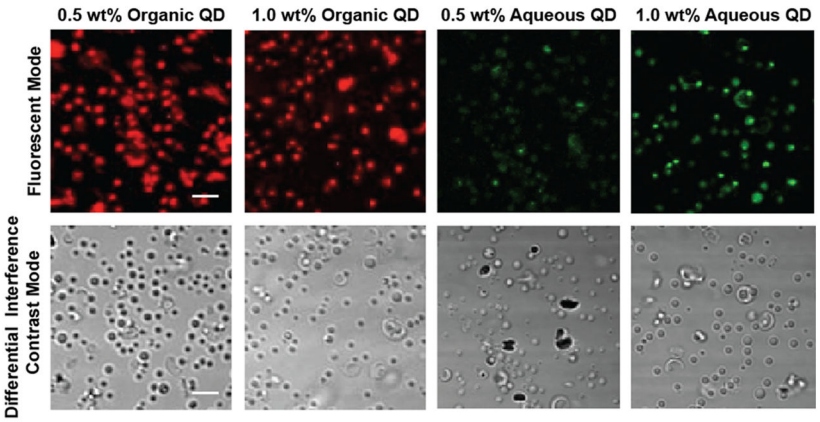

Figure 5.

Fluorescent confocal microscopy images of QD-MB. Concentration is 1 mg/mL. The scale bar is the same in each panel and is 5 μm.

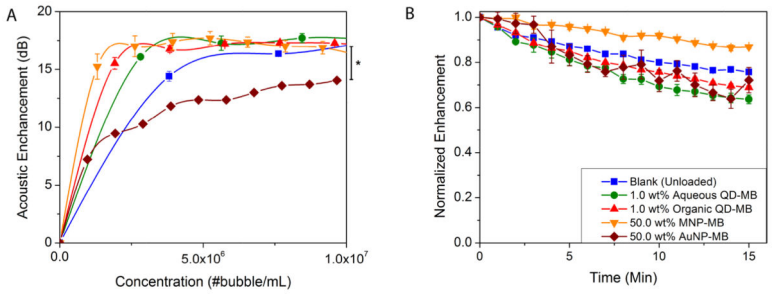

Figure 6.

Acoustic evaluation of MB. (A) Effect of MB dose and nanoparticle loading on acoustic enhancement by each high loading agent. (B) Acoustic stability of each agent. (A significant decrease in *in vitro* enhancement was seen in 50.0 wt % AuNP-MB relative to the unloaded control $*p = 0.0130$.)

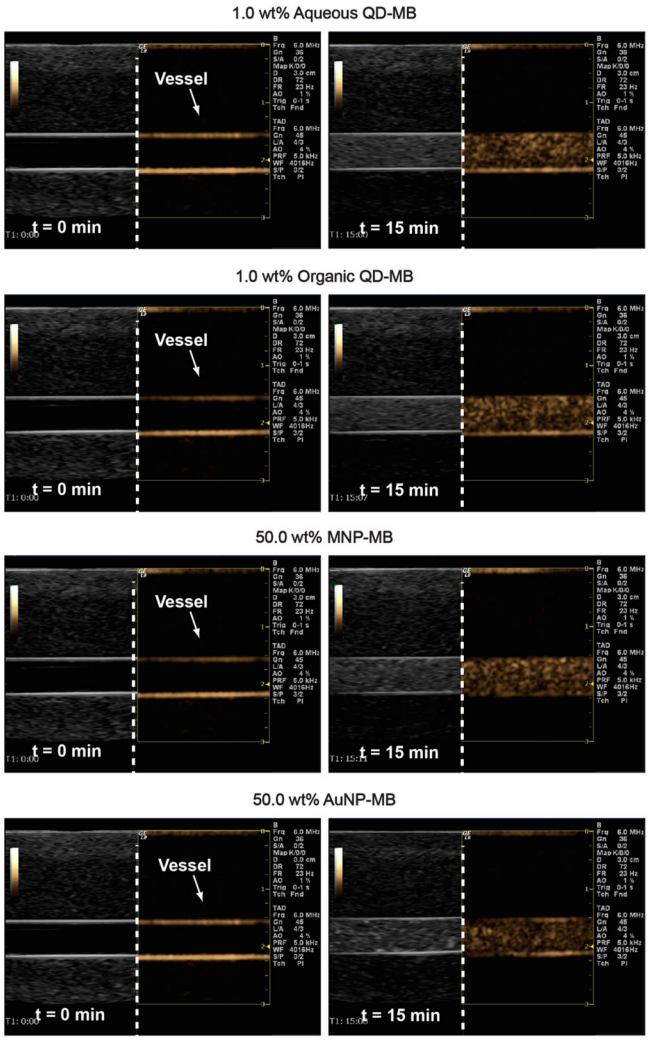

Figure 7.

In vitro ultrasound enhancement of nanoparticle loaded MB in a flow phantom using a commercial ultrasound scanner at baseline (left) and 15 min postinjection (right).

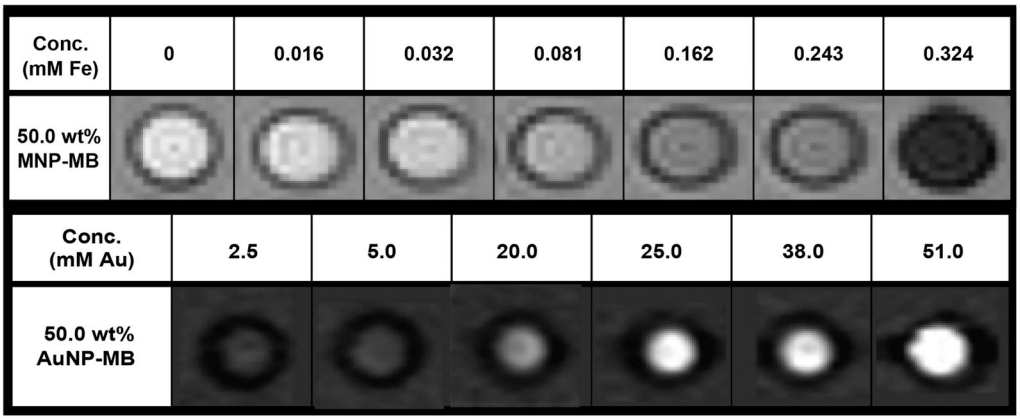

Figure 8.

Upper row: MR images of MNP-MB phantom (50.0 wt %) acquired at 3T. Lower row: CT images of a phantom containing AuNP-MB (50.0 wt %) acquired at 100 kV. Attenuation range is from −100 to 450 HU.

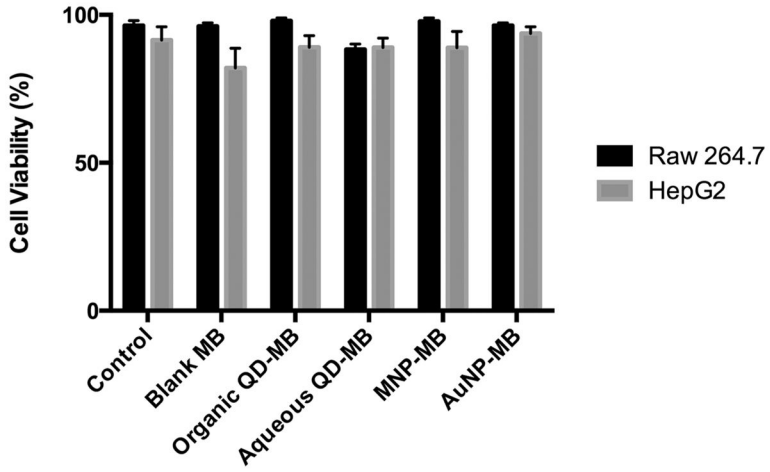

Figure 9.

Viability of RAW 264.7 and HepG2 cell lines incubated for 4 h with nanocrystal loaded MB, blank MB, and media only (control).

Table 1

Summary of Nanoparticle Loading Weight Percentages Used in the Study[a]

	low loading wt %	high loading wt %
control	0 wt %	
aqueous QD-MB	0.5 wt %	1.0 wt %
organic QD-MB	0.5 wt %	1.0 wt %
MNP-MB	33.3 wt %	50.0 wt %
AuNP-MB	33.3 wt %	50.0 wt %

[a]Values are given as total nanoparticle weight as a percentage of the PLA polymer used.

Table 2

Summary of Nanoparticle Properties

name	organic QD	aqueous QD	MNP	AuNP
type	CdS	CdSe	Fe_3O_4	Au
source	purchased from NN-Laboratories	purchased from Ocean NanoTech	in-house; coprecipitation	in-house; two-phase reduction
emission peak (nm)	460	580		
average size (nm)	5.5	4	10	3
capping agent	oleic acid	mercaptopropionic acid	oleic acid	dodecanethiol
solvent	methylene chloride	water	methylene chloride	

Table 3

Effects of Nanoparticle Loading on Microbubble Size, PDI, ζ, and Concentration

	microbubble size (nm)	PDI	zeta potential (mV)	MB concentration (mg)
control	2216 ± 59	0.192 ± 0.03	−24.7 ± 1.6	$2.50 \times 10^9 \pm 1.83 \times 10^8$
1.0 wt % aqueous QD-MB	2734 ± 200	0.201 ± 0.04	−26.3 ± 0.5	$1.26 \times 10^9 \pm 2.91 \times 10^8$
1.0 wt % organic QD-MB	2259 ± 55	0.209 ± 0.01	−22.3 ± 2.9	$1.85 \times 10^9 \pm 2.89 \times 10^8$
50.0 wt % MNP-MB	2396 ± 196	0.217 ± 0.02	−20.8 ± 0.7	$8.60 \times 10^8 \pm 4.49 \times 10^7$
50.0 wt % AuNP-MB	1653 ± 57[a]	0.267 ± 0.03	−28.9 ± 1.9	$6.35 \times 10^8 \pm 1.13 \times 10^8$

[a] $p = 0.0213 < 0.05$.

Table 4

Percentages of Yield, Loading, and Encapsulation Efficiency of Different Nanoparticles

samples	50.0 wt % MNP	50.0 wt % AuNP	1.0 wt % aqueous QD	1.0 wt % organic QD
wt % yield	62.5% ± 0.50	81.55% ± 0.95	79.9% ± 7.82	82.5% ± 3.86
wt % loading	22.19% ± 7.21	23.34% ± 2.74	0.15% ± 0.02	0.29% ± 0.05
wt % encapsulation efficiency	27.79% ± 6.59	38.03% ± 2.71	10.50% ± 0.65	25.62% ± 1.58